Nuclear Inst. and Methods in Physics Research B xxx (xxxx) xxx–xxx

Contents lists available at ScienceDirect

Nuclear Inst. and Methods in Physics Research B

journal homepage: www.elsevier.com/locate/nimb

Mass spectrometric investigation of material sputtered under swift heavy ion bombardment

L. Breuer[a], P. Ernst[a], M. Herder[a], F. Meinerzhagen[a], M. Bender[b], D. Severin[b], A. Wucher[a,*]

[a] Fakultät für Physik, Universität Duisburg-Essen, 47048 Duisburg, Germany
[b] GSI Helmholtz Zentrum für Schwerionenforschung, 64291 Darmstadt, Germany

A B S T R A C T

The flux of particles emitted from a solid surface under electronic sputtering conditions induced by irradiation with Swift Heavy Ions (SHI) was investigated using time-of-flight mass spectrometry in connection with laser post-ionization. While secondary ions emitted from the irradiated surface were directly detected using a reflectron ToF spectrometer, the corresponding neutral particles were post-ionized after their emission using single photon ionization in a pulsed VUV laser beam. The ToF spectrometer was operated in delayed extraction mode, thereby ensuring that secondary ions and post-ionized neutrals were detected under otherwise identical experimental conditions. For comparison with a purely nuclear sputtering process, spectra taken under irradiation with 4.8 MeV/u $^{197}Au^{26+}$ and $^{48}Ca^{10+}$ ions were compared to those measured *in situ* under bombardment with 5 keV Ar^+ ions. Most importantly, we find that in most cases the vast majority of the sputtered material is emitted in the neutral state, with the flux of sputtered particles mainly consisting of single atoms and small (mostly diatomic) clusters. For metallic targets, we find a significant electronic sputtering effect for In and Bi, while other metals like Mo or Ag do not appear to sputter very efficiently under SHI irradiation. As an example for a semiconductor target, (amorphous) Ge is found to exhibit a large electronic sputtering yield under irradiation with Au projectiles, while practically no effect is observed with the Ca ions, thereby clearly indicating a stopping power threshold for this material. KBr as an example for an ionic crystal exhibits the expected large yield, with the sputtered material mainly consisting of atomic species and neutral KBr and K_2Br clusters. We find about equal signals of neutral and ionized K atoms and K_2Br clusters, while KBr is exclusively detected as a neutral molecule. Besides these major species, we find a progression of $[KBr]_nK^+$ and – with much smaller intensity – $[KBr]_nBr^-$ clusters, which exhibits a similar size distribution as observed by others for $[LiF]_nLi^+$ clusters emitted from LiF. Interestingly, no negative halogen ions are observed under SHI irradiation, while they are clearly detected under nuclear sputtering conditions with similar intensity as the corresponding positive alkali ions.

1. Introduction

If a solid is subjected to irradiation with energetic heavy ions, particles may be released from the surface, a process which is generally termed “sputtering”. Depending on the projectile energy, there are two distinct regimes with different fundamental mechanisms underlying the sputtering process. At low impact energy, the projectile transfers energy to the solid predominantly via (mostly elastic) collisions with the target atoms (“nuclear stopping”), which then may undergo further collisions, thereby generating more recoils etc. As a consequence, a collision cascade develops which may knock particles off the surface once their recoil energy exceeds the surface binding energy. In the following, this process will be referred to as “collisional sputtering”. In the limit of high impact energy, on the other hand, the primary energy transfer proceeds in form of electronic stopping of the projectile, leading to a strong, temporal and local electronic excitation which may then feed energy into the lattice system via electron-phonon coupling. Again, the process may lead to the emission of particles, a process which in the following will be referred to as “electronic sputtering”. Both sputtering processes have been extensively studied in the past, and much of the related experimental and theoretical work performed to unravel the fundamental mechanisms governing the particle emission process has been reviewed in a series of dedicated monographs [1].

Up to date, the microscopic dynamics of a sputtering process is only accessible via model calculations. Experimental access is still restricted to asymptotic states, where the flux of emitted particles is characterized

* Corresponding author.
E-mail address: andreas.wucher@uni-due.de (A. Wucher).

http://dx.doi.org/10.1016/j.nimb.2017.10.019
Received 21 July 2017; Accepted 19 October 2017

via observables like the sputter yield, i.e., the total number of particles that is on average emitted per projectile impact, as well as their distribution with respect to species, charge or excitation state, emission velocity and angle, etc., which can be predicted by the model calculations. While the total sputter yield is relatively easy to measure – for instance via weight loss or collector techniques – quantitative information regarding the composition of the sputtered flux requires a measurement of the partial sputter yields of different emitted species. One way to obtain such information is mass spectrometry, which, however, requires the investigated particles to be electrically charged. Secondary Ion Mass Spectrometry (SIMS) has therefore emerged as a widely used tool to identify atomic and molecular species desorbed from a solid surface under "primary" ion bombardment particularly in the nuclear sputtering regime [2], and numerous applications of the technique both with respect to fundamental research and practical surface analysis have been published. In connection with sophisticated models based, for instance, on molecular dynamics computer simulations, the collisional sputtering process is now fairly well understood [3,4].

The electronic sputtering process induced by an SHI impact, on the other hand, appears to be less well characterized [5]. While total yields and angular distributions of the sputtered material have been collected using the catcher technique for a few ion-target combinations [5–16] and systematic trends regarding their correlation with projectile charge state, velocity and electronic stopping power have been identified [5], much less is known about the composition of the material sputtered under SHI irradiation. Collector-type experiments can be used to determine the stoichiometry of the sputtered flux – even as a function of the emission angle – but the results do not reveal information regarding the emitted particles. For multicomponent targets, the sample is sometimes found to be sputtered stoichiometrically, in other cases strong preferential sputtering effects are observed, leading to the enrichment of one or more components at the irradiated surface [15]. Even for single component targets, one of the fundamental open questions regards the role of cluster emission, i.e., the fraction of the sputtered material that is emitted in form of molecules or clusters as opposed to single atoms. In some cases, information of this kind was deduced from a microscopic analysis of the material deposited on a collector foil [5], but it is unclear whether the observed nanostructure really is determined by the composition of the deposited material or rather by its mobility at the catcher surface. In a number of other studies, SIMS was used to analyze the ionized part of the sputtered flux [17–39]. Many of these studies were focused on the electronic sputtering process induced by SHI impact onto lithium fluoride, and time-of-flight (ToF) techniques were used to determine the emission velocity and angle distributions of the emitted secondary ions [28,30,31,34,36,37]. The resulting distributions have been interpreted in terms of model calculations based on the dynamical charge distribution in an SHI induced track [40] and may therefore be specific for emitted ionic species.

A fundamental problem regarding the mass spectrometric characterization of a sputtering process is the fact that most of the sputtered material is emitted in a neutral charge state. While this is known from the catcher experiments, questions like, for instance, the cluster distribution within the sputtered flux cannot be answered without the mass resolved detection of the sputtered neutral species. Moreover, both the velocity and angle distributions of emitted secondary ions may in principle be affected by a velocity or trajectory dependent ionization probability of a sputtered particle. The emission velocity spectrum of sputtered neutral material can in principle be measured by the catcher technique in connection with a mechanical time-of-flight analysis [41,42], but again there is no resolution with respect to the emitted particles. In the past, we have therefore developed a technique to detect sputtered neutral particles via laser induced post-ionization subsequent to their emission from the ion irradiated surface, which was used to unravel the emission and ionization process of particles emitted under collisional sputtering conditions [43]. We have recently adapted this Secondary Neutral Mass Spectroscopy (SNMS) method to the M1 beamline at GSI, thereby allowing to analyze the material sputtered under SHI bombardment and compare the results with those obtained under collisional sputtering conditions. Here, we present data obtained with this system for irradiation of In, Bi, Ge and KBr targets with 4.8 MeV/u gold and calcium ions.

2. Experimental

The experiments were performed using a home-built reflectron time-of-flight (ToF) mass spectrometer installed at the M1 beam line of the UNILAC accelerator facility at the Helmholtz centre for heavy ion research (GSI) in Darmstadt, Germany. The system has been described in detail elsewhere [44], and therefore only a brief description of the relevant features will be given here. The ToF spectrometer is mounted under 45° with respect to the UNILAC ion beam, and the sample is positioned perpendicular to its ion optical axis so that the projectile ions strike the sample under 45° with respect to the surface normal. For reference and alignment purposes, the system also includes a 5 keV argon ion beam which impinges under the same polar angle, albeit with a 45° rotated azimuth with respect to the surface normal. Swift heavy projectile ions used in these experiments were ^{197}Au and ^{48}Ca ions of a selected charge state (26+ for Au and 10+ for Ca) delivered by the accelerator with a specific energy of 4.8 MeV/u. We note that these conditions do not coincide with the equilibrium charge state, which is reached once the projectile penetrates a distance of typically several 100 nm into the solid, and therefore the energy deposition from electronic stopping of the projectile will vary as a function of penetration depth [45]. For the sputtering process investigated here, however, this variation is irrelevant since the mean emission depth of sputtered particles is only of the order of several nm. The UNILAC beam was shaped to a spot profile of typically about 6 mm diameter using a fluorescent target in place of the sample. The spot profile of the keV-beam was also examined by the fluorescent target and set to a diameter of about 2 mm FWHM.

Secondary ions released from the surface were extracted into the ToF spectrometer using a pulsed extraction field generated by switching the sample to a potential of +1600 V with respect to ground. The switching was done using a fast HV switch (Behlke HTS 31 GSM) with a rise time of about 20 ns, with the switching time marking the flight time zero for the detected ions. The reflector voltage (1450 V) was tuned slightly below the target potential (1600 V) in order to ensure that only ions originating from a minimum height of about 1 mm above the sample surface could be reflected and detected. In connection with the flight time refocusing properties of the ToF spectrometer, this determined a sensitive volume of about 1 mm diameter located at about 1 mm above the surface and centered around the ion optical axis of the spectrometer, from which ions could be extracted and contribute to the detected sharp flight time peaks [43].

Secondary neutral particles emerging from the bombarded surface were post-ionized using a pulsed F_2 laser operated at a VUV wavelength of 157 nm. The corresponding photon energy of about 8 eV ensured that neutral atoms and molecules possessing ionization potentials up to this value could be efficiently post-ionized via non resonant single photon absorption. The laser beam was directed parallel to the sample surface at a distance matching the location of the ToF sensitive volume. The beam was focused to a spot diameter of about 1 mm using a 250 mm focal length CaF_2 lens, which at the same time acted as the entrance window to the ultrahigh vacuum chamber housing the experiment. The laser delivered output pulses of about 4–7 ns duration and up to about 1.6 mJ pulse energy, which was monitored using its internal energy monitor and calibrated using a GenTech power meter. Due to geometrical restrictions, the laser beam had to be guided through an evacuated beam line of about 2 m length and then coupled into the vacuum system via a ~120° deflecting mirror, both leading to a significant

intensity loss before being introduced the experiment chamber. The intensity of the laser pulse actually entering the vacuum chamber was therefore monitored again with a fast in-vacuum photoelectric detector, which could also be used in order to control the timing of the pulse.

During most of the experiments, the laser pulse was fired simultaneously with the ion extraction pulse. This way, the instrument cannot distinguish between intrinsic secondary ions and post-ionized neutral particles of the same species, thereby detecting both entities under otherwise the same experimental conditions. In order to distinguish between secondary ions and post-ionized neutrals, spectra were therefore taken with and without firing the laser beam. Since the projectile ion pulses delivered by the UNILAC have a duration of the order of several milliseconds, several ToF spectra were taken during one UNILAC pulse at the maximum possible repetition rate of up to 10 kHz (depending on the acquired mass range). Since the post-ionization laser can only sustain a limited repetition rate, it was only fired during the first spectrum of such a burst, the data of which was then added to the SNMS spectrum, leaving the remaining spectra to be added to the corresponding SIMS spectrum. Note that the SNMS spectra acquired this way contain the secondary ion as well as the post-ionized secondary neutral signals, so that the data corresponding to the secondary neutral particles alone must be derived by subtracting the corresponding SIMS spectrum. In some of the experiments, the post-ionization laser pulse was therefore delayed with respect to the firing of the ion extraction pulse. This way, the laser pulse now marks the flight time zero for the post-ionized neutrals, thereby shifting the photoion pulses in the ToF spectrum with respect to the SIMS pulses and allowing a clear differentiation between both signals. This technique, which is very useful for simple mass spectra, may greatly complicate the spectra measured for more complex samples and was therefore only used scarcely.

Inbetween subsequent UNILAC pulses, additional spectra were measured either with the keV Argon ion beam bombarding the surface or without any ion bombardment at all. While the first deliver reference spectra which allow a direct comparison between electronic and nuclear sputtering processes, the latter are needed to ensure that the measured signals are actually related to the ion bombardment. In particular, the data taken with the laser beam alone reveal important information about the background signal arising from laser photoionization of residual gas components. All six spectra (MeV-SNMS, MeV-SIMS, keV-SNMS, keV-SIMS, residual gas and blank spectra) were obtained in a highly interleaved manner during a single UNILAC pulse cycle and summed over a desired number of such cycles in order to achieve the targeted counting statistics. Since the signal measured in these experiments is proportional to the momentary pulse particle current, i.e., the number of arriving projectile ions per unit time (which will be given in nanoampere equivalents in the remainder of this paper), it is important to know the temporal pulse current profile of the UNILAC pulses in order to correlate the interleaved spectra. One way to obtain that information is by monitoring the momentary pulse current of each single pulse using a respective monitor signal generated by the accelerator. Another technique applied here is to introduce a controllable delay between the data acquisition gate and the UNILAC pulse. This way, both the secondary neutral and ion signals can be measured as a function of time during a single SHI pulse, a feature which provides an intrinsic way to determine the UNILAC pulse profile and also becomes important in the discussion of the measured signals below.

After passing the Tof spectrometer, secondary ions and post-ionized neutral particles were detected using a Chevron stack of two microchannel plates (MCP) equipped with a grounded entrance grid. A post-acceleration voltage of 4 kV was applied between the grid and the MCP front, which in connection with the sample bias of 1600 leads to a total ion impact energy of 5.6 keV onto the detector. The MCP output current was measured on a collector plate biased at +45 V with respect to the MCP rear and digitized using a fast transient digitizer board (Signatec PX 1500). The 8 bit digitizer delivers bit values between 0 and 255, which will in the following be called “ct” and correspond to voltages between 0 and 500 mV measured at a 50 Ω termination resistor. Note that the unit of 1 ct defined this way does not correspond to the registration of one ion (as is, for instance, the case in flight time spectra acquired using a time-to-digital converter). In order to determine the actual number of detected ions of a particular mass, the corresponding flight time peak must be integrated, and the resulting integral must be divided by the average peak integral induced by a single ion impact. In many cases, the data were summed over many acquired spectra (“reps”). To allow an easy comparison, the measured signal will in the following be normalized to the number of reps and displayed in units of “cts/rep”.

Each investigated sample was first analyzed as introduced into the vacuum chamber. The ion fluence applied during a single UNILAC pulse varied depending on the UNILAC pulse current and duration, with the latter being selected by the accelerator facility and not changeable by us. The total fluence applied during a single UNILAC pulse therefore varied between 10^7 and 10^8 ions/cm^2. Depending on the number of pulse cycles used to acquire the data, the SHI fluence applied during acquisition of one spectrum therefore varied between approximately 10^8 and 10^{11} ions/cm^2. In order to examine the influence of the applied total fluence, pseudo depth profiles were usually measured where spectral data was taken repetitiously without applying additional ion bombardment inbetween. In some of the experiments, the sample was sputter cleaned either prior to or during the data acquisition using dc bombardment with the keV argon ion beam. In particular for those cases where utmost surface cleanliness was desired, the Ar^+ beam was interleaved with the data acquisition, leaving it on dc operation and only temporarily pulsing it off during the acquisition gates for UNILAC and blank spectra, respectively.

Metal samples were made from thick polycrystalline foils of indium and bismuth (Goodfellow), germanium samples were cut from an undoped Ge wafer, and KBr samples were produced by cleaving a KBr single crystal (Korth Kristalle GmbH). All samples were introduced as is, with the metal and Ge samples being sonicated in isopropanol for a few minutes before mounting on the sample holder. All samples were either glued to the sample holder using copper tape or clamped with a Mo mask.

3. Results and discussion

3.1. Metallic targets

The six spectra that were simultaneously acquired on a sputter precleaned indium sample are shown in Fig. 1. Prior to the acquisition of the spectra, the sample was bombarded with the keV ion beam operated in dc mode for 20 s, thereby applying a total Ar^+ ion fluence of about 8×10^{14} ions/cm^2 and removing a surface layer of several nm thickness. The spectra are labeled according to the acronyms MeV, keV, SNMS, SIMS and Blank, where MeV, keV and Blank denote spectra that were acquired with either the UNILAC beam, the keV ion beam or without any ion beam, respectively, and SNMS and SIMS denote spectra obtained with or without firing the post-ionization laser. Note that the SNMS spectra always contain the SIMS spectrum as well, so that the true spectrum of post-ionized secondary neutral particles is obtained by subtracting the SIMS background from the respective SNMS spectrum.

First, it is seen that both blank spectra taken with and without firing the post-ionization laser, but without any ion bombardment (right panels), are empty. This observation is important since it *i*) ensures that the rather complicated sorting scheme correlating the different interleaved data sets with the corresponding spectra works correctly and *ii*) reveals that the background signal generated by laser ionization of the residual gas is negligible. Since this was the case for all of the data sets displayed in the remainder of this paper, the blank spectra will in the following be omitted.

Two observations are striking when looking at the data presented in

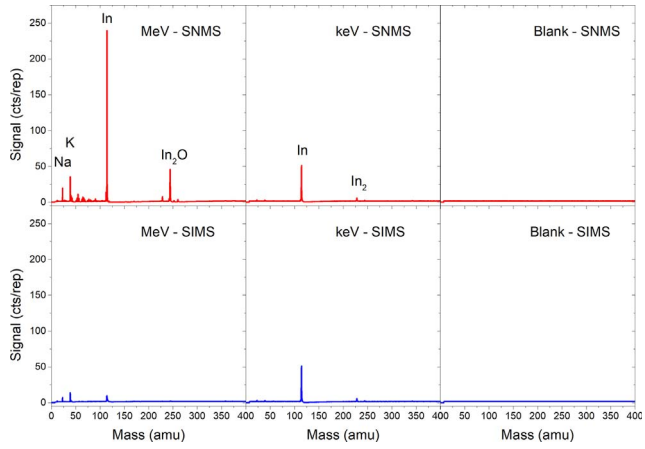

Fig. 1. SNMS and SIMS spectra taken on a sputter pre-cleaned indium sample under 4.8 MeV/u $^{197}Au^{26+}$ impact (left panels), 5 keV Ar^+ impact (middle panels) and without ion bombardment (right panels). The data were taken using a pulse particle current of 15 nA (SHI, flux density ~3×10^{11} ions/cm^{2}s) and 50 nA (Ar^+), respectively. All spectra were acquired simultaneously using a total MeV and keV ion fluence of 1.6×10^{10} ions/cm^2.

Fig. 1. First, and probably most important, it is seen that the secondary ion signal measured under SHI irradiation is small compared to that of post-ionized neutral particles. Although we do not exactly know the post-ionization efficiency, this observation clearly shows that most of the material sputtered from the indium sample irradiated under these conditions must be neutral. In fact, the ratio between the secondary neutral and ion signals which can be extracted for every sputtered species separately must be regarded as a lower limit of the true neutral-to-ion ratio, since the neutral signal can only be underestimated by incomplete post-ionization. If the laser intensity would be sufficient to warrant saturation of the photoionization probability across the entire sensitive volume, the measured ion-to-neutral ratio would directly represent the ionization probability, i.e., the probability of a sputtered species to be emitted in a charged state and form a secondary ion. Unfortunately, the laser employed in these experiments is not powerful enough to ensure these conditions. Since a more powerful system cannot be installed at the GSI beam line due to space restrictions, the ability to measure the corresponding spectra generated under keV ion bombardment becomes particularly important, since it delivers relative information about the ion-to-neutral signal ratio measured under both irradiation conditions. The keV experiment, on the other hand, can easily be repeated in our lab at Duisburg, where we have a more powerful F_2 - Laser installed on a practically identical ToF spectrometer, thereby ensuring saturation ionization conditions which allow an absolute calibration of the measured relative ionization probabilities.

The second important observation made in Fig. 1 is that the signals measured under keV bombardment are smaller than those measured under SHI irradiation. In connection with the fact that the SHI spectra were taken with a smaller pulse projectile current, this observation indicates the (neutral) sputter yield induced under SHI impact to be larger than that induced by 5 keV Ar^+ ion impact. Estimating the latter using the SRIM program package [46], one arrives at a keV induced sputter yield of 8.6 atoms/ion, indicating that the SHI-induced yield must be significantly larger. Normalizing, for instance, the measured signal of neutral In atoms to the equivalent pulse particle current, one arrives at an MeV/keV ratio of about 17, indicating an apparent sputter yield of more than 100 atoms/ion under irradiation with 4.8 MeV $^{197}Au^{26+}$ ions. There are, however, a few potential errors that make the interpretation of the measured signal ratio in terms of relative sputtering yields difficult. First, a possible heating of the sample by the SHI irradiation needs to be taken into account. If the sample temperature rises to values close to the critical temperature of the target material, at least part of the signal measured under MeV bombardment might simply be induced by thermal evaporation. In this context, we note that the spectrum in Fig. 1 was measured with an UNILAC spot diameter of about 6 mm, yielding a projectile ion flux density of about 3×10^{11} ions/cm^{2}s. For a 946 MeV projectile ion, this results in a power density of about 50 W/cm^2, which is deposited into the target during an UNILAC pulse of 1 ms duration. In connection with the relatively low UNILAC repetition rate used in these experiments (2 Hz), we believe that the average energy deposition rate of about 100 mW will not lead to a significant overall heating of the target. There might, in principle, be a transient heating effect, leading to a temporal temperature increase in the course of a single projectile pulse, which then cools down again during the pause between subsequent pulses. In fact, we have observed such an effect by looking at the temporal evolution of signals measured for neutral and ionized molecules sputtered from a thin organic film deposited on a silicon substrate [47]. In this case, the molecular secondary ion signal strictly followed the UNILAC pulse projectile current, whereas the neutral molecules developed an additional signal contribution which increased with time during the ion pulse and decayed exponentially after the end of the pulse. In the present case of a thick metallic target mounted on a metallic sample holder, however, both the secondary ion and neutral signals are found to exactly follow UNILAC pulse current profile, so that we consider the temperature increase during the pulsed SHI irradiation to be negligible. Moreover, we have repeated the same experiment using a much lower ion flux density of 7×10^9 ions/cm^{2}s and still found a significantly larger In^0 signal under MeV impact than under keV bombardment.

A second potential error is related to the fact that that the MeV and keV ion beams have different focus conditions, so that the measured signal may in principle arise from different areas on the irradiated surface. In order to investigate this further, data were taken as a function of the aperture diameter of the molybdenum metal mask covering the indium surface. As an example, Fig. 2 shows data that were taken with a 4.8 MeV/u $^{48}Ca^{10+}$ beam.

Interestingly, the In^0 signal generated by the SHI beam is now smaller than that generated by the keV ion beam, although the pulse particle current is about two times larger than that of the gold ion pulses in Fig. 1, indicating that the sputter yield induced by impact of a 4.8 MeV/u $_{48}Ca^{10+}$ must be smaller than that induced by 5 keV Ar^+ bombardment. The Mo^0 signal observed under keV bombardment as well as the strong K^0 and K^+ signals observed under both bombarding conditions originate from sputtering of the molybdenum mask and therefore become weaker with increasing aperture diameter. The signal increase observed for the In^0 signal measured under keV bombardment reveals that 44%, 72% and ~100% of this signal are generated from the

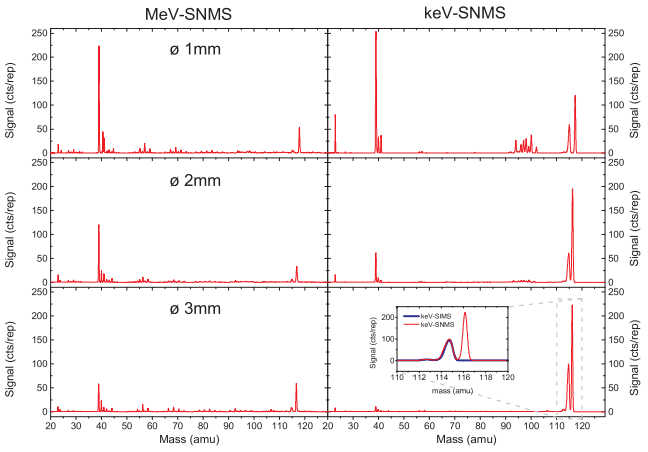

Fig. 2. SNMS spectra taken on an indium surface covered by a molybdenum mask with a 1 mm (left), 2 mm (center) or 3 mm diameter central aperture. The data were acquired under 4.8 MeV/u $^{48}Ca^{10+}$ impact at a pulse particle current of about 30 nA (SHI, flux density ~6×10^{11} ions/cm^{2}s) and 75 nA (Ar^+), respectively.

central 1, 2 and 3 mm diameter spots on the irradiated surface, respectively. This finding can be interpreted in terms of a Gaussian distribution of about 2 mm FWHM, which arises from the convolution of the keV ion beam profile and the lateral sensitivity distribution of the mass spectrometer. In contrast, the In^0 signal measured under SHI irradiation is practically independent of the aperture diameter, indicating that nearly all of the signal measured under these bombarding conditions must arise from the central spot of 1 mm diameter. This difference can only be understood in terms of the emission angle distribution of the sputtered particles, which under SHI bombardment must apparently be more forward directed along the surface normal than under keV bombardment. This interpretation would be consistent with angular distribution measurements performed using the catcher technique, which reveal a forward peaked emission distribution for metallic surfaces as well [5,11]. Moreover, a detailed inspection of the flight time peak shapes observed in the data of Fig. 2 indicates that the secondary neutral atoms ejected under SHI bombardment may on average be emitted with lower velocity than those ejected under nuclear sputtering conditions. Details of this analysis are outside the scope of this work and will be published in a different paper, but we note that this notion would be consistent with measured emission energy distributions of Li^+ secondary ions emitted from lithium fluoride [35]. Since our experiment is sensitive to the *number density* of sputtered particles within the sensitive volume of the spectrometer (rather than their *flux*), both findings would act to enhance the SHI generated signal with respect to that measured under keV bombardment conditions, leading to an overestimation of the corresponding sputter yield. Clearly, more detailed investigations of the emission angle and energy distributions of sputtered neutral particles are needed in order to quantitatively convert the measured signals into sputter yields.

In any case, the data presented in Figs. 1 and 2 clearly reveal a sizeable sputtering yield under SHI bombardment of indium. Calculating the purely nuclear sputtering contribution using SRIM, one finds a yield of 0.57 atoms/ion for 4.8 MeV/u Au irradiation, which is negligibly small compared to that calculated for 5 keV Ar^+ bombardment. From the data presented here, we therefore conclude that there must be a clear electronic sputtering effect under bombardment of indium with 4.8 MeV/u Au^{26+} projectiles, which is smaller but still visible for 4.8 MeV/u $^{48}Ca^{10+}$ projectiles as well.

At first sight, the observation of electronic sputtering for a metallic sample appears surprising, since it is a common notion that such effects should be small for such targets. In fact, we find only relatively small SHI induced signals for good conducting metals like silver and molybdenum (see Fig. 2, where the molybdenum specific signals are absent in the MeV generated spectra). There are, however, other metals which show significant electronic sputtering as well. As an example, data measured on a polycrystalline bismuth sample irradiated with 4.8 MeV/u $^{197}Au^{26+}$ ions are shown in Fig. 3. Also in this case, we find large SHI generated signals, which are much stronger than those observed under keV ion bombardment. Moreover, the neutral-to-ion ratio observed for Bi atoms and Bi_2 clusters is even larger than that observed for the indium target, showing that also in this case the vast majority of the sputtered material is neutral. The relatively large signal observed for neutral Bi_2 clusters is another good indication that the sputtered particles are not emitted by thermal evaporation, because in that case one would predominantly expect the emission of neutral atoms.

Apparently, both indium and bismuth exhibit large electronic sputtering yields under 4.8 MeV/u Au^{26+} projectile bombardment, while other metals such as molybdenum or silver do not. The collisional sputter yield under 5 keV Ar^+ bombardment, on the other hand, is comparable for these metals.

At present, we can only speculate about the reason behind these observations. A relevant target property which is known to critically influence sputtering yields is the surface binding energy, which is often approximated by the sublimation energy of the bulk material. Interestingly, this quantity is quite similar for indium (2.6 eV), bismuth

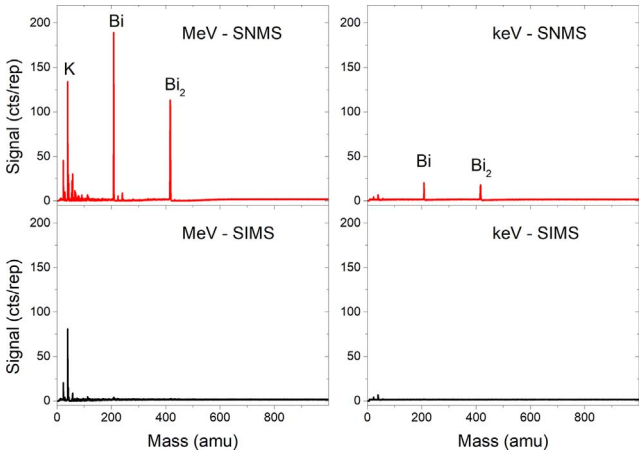

Fig. 3. SNMS and SIMS spectra taken on a freshly introduced bismuth sample under 4.8 MeV/u $^{197}Au^{26+}$ impact (left panels) and 5 keV Ar^+ impact (right panels). The data were taken using a pulse particle current of 15 nA (SHI, flux density $\sim 3 \times 10^{11}$ ions/cm^{2}s) and 50 nA (Ar^+), respectively. All spectra were acquired simultaneously with a total MeV and keV ion fluence of 1.6×10^{10} ions/cm^2.

(2.15 eV) and silver (2.96 eV). What is fundamentally different, however, is the melting temperature, which is low for In (157 °C) and Bi (271 °C) and high for Ag (962 °C) or Mo (2623 °C). Therefore, a molten track is more readily formed, where the material is in an amorphous state, thereby slowing down the transport of electronic excitation energy and, hence, the cooling of the track volume. Also, both In and particularly the semi-metal Bi exhibit a significantly lower electrical conductance than Ag, so that maybe even the electronic heat diffusivity of the pristine crystalline material is lower in these metals, leading to more efficient trapping of the primary electronic excitation and, hence, higher lattice heating via electron-phonon coupling. Clearly, more data are needed to clarify this point.

3.2. Semiconductor targets

As an example for a semiconducting target material, germanium was investigated since the ionization potential of Ge atoms (7.88 eV) is just below the photon energy of our ionization laser and therefore allows efficient detection of sputtered Ge atoms as well as Ge_n clusters via single photon ionization [48]. Fig. 4 shows data that were taken on a freshly introduced sample. One can immediately see that the MeV ion

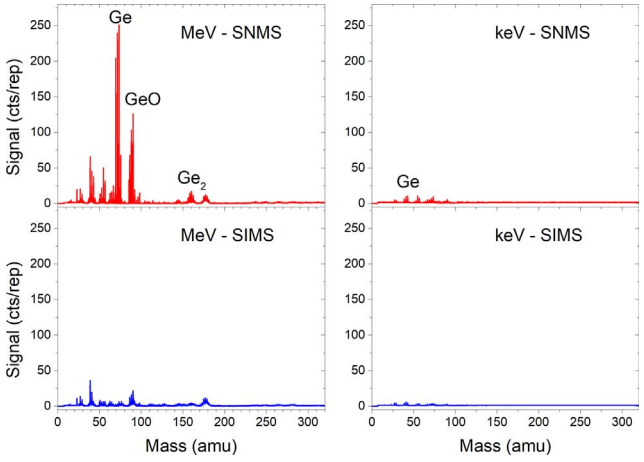

Fig. 4. SNMS and SIMS spectra taken on a freshly introduced germanium sample under 4.8 MeV/u $^{197}Au^{26+}$ impact (left panels) and 5 keV Ar^+ impact (right panels). The data were taken using a pulse particle current of 15 nA (SHI) and 50 nA (Ar^+), respectively, with a total MeV and keV ion fluence of about 1.6×10^{10} ions/cm^2 applied per spectrum in both cases.

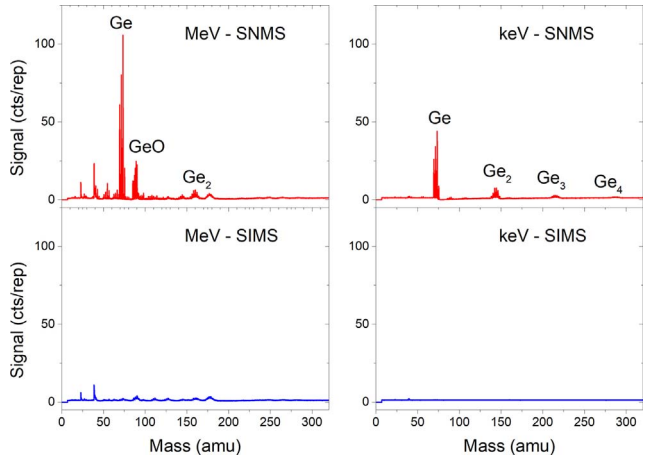

Fig. 5. SNMS and SIMS spectra taken on a sputter pre-cleaned germanium sample under 4.8 MeV/u $^{197}Au^{26+}$ impact (left panels) and 5 keV Ar^+ impact (right panels). The data were taken using a pulse particle current of 15 nA (SHI) and 50 nA (Ar^+), respectively, with a total ion fluence of about 1.6×10^{10} ions/cm^2 applied per spectrum in both cases. The total Ar^+ ion fluence applied during the pre-cleaning process was of the order of 10^{16} ions/cm^2.

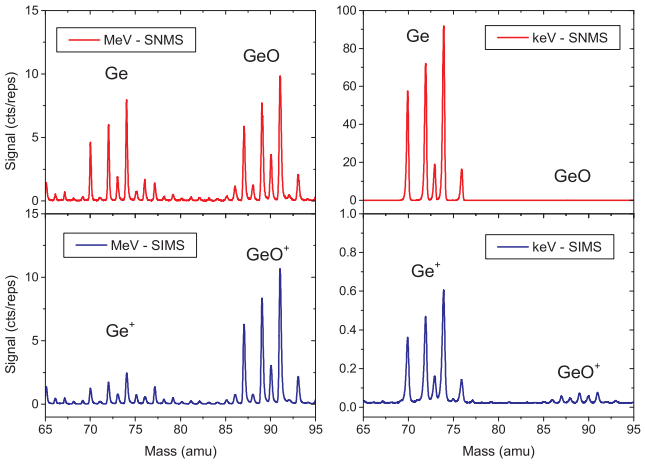

Fig. 6. SNMS and SIMS spectra taken on a dynamically sputter cleaned germanium sample under 4.8 MeV/u $^{197}Au^{26+}$ impact (left panels) and 5 keV Ar^+ impact (right panels). The spectra were taken using a pulse particle current of 1.1 nA (SHI) and 75 nA (Ar^+), respectively, with an interleaved dc Ar^+ ion bombardment at about 4×10^{13} ions/cm^{2}s as described in the text.

beam generates a rich spectrum, again clearly dominated by post-ionized sputtered neutral species, while the spectra generated by the keV ion beam are comparably empty. If the surface is sputter cleaned by operating the 5 keV Ar^+ ion beam in dc mode for several minutes, thereby applying a keV ion fluence of the order of 10^{16} ions/cm^2 and removing a surface layer of several nm thickness, one obtains the spectra shown in Fig. 5. While the SHI generated spectrum exhibits only slight changes, the keV generated spectra now clearly show sputtered neutral Ge atoms and a series of Ge_n clusters as observed previously [48]. In principle, this change is expected, since it is well known that under keV bombarding conditions the vast majority of sputtered particles originates from the uppermost surface layer. Therefore, it is understandable that the spectrum generated under these conditions strongly depends on any surface contamination which will effectively suppress particularly the sputtered neutral particle signal arising from the underlying substrate material. Therefore, these signals are often found to strongly rise upon dc sputter cleaning. It is interesting to note that this dependence is much weaker in the spectra measured under SHI irradiation.

Moreover, there are other interesting differences between the spectra generated by SHI and keV ions, respectively. First, we note that the SHI generated spectrum taken on both the pristine and the sputter cleaned surface contains a sizeable fraction of GeO and GeOH molecules, while these signals are practically absent in keV generated spectrum of the sputter pre-cleaned sample. Moreover, germanium dimers sputtered under SHI impact are predominantly detected in form of Ge_2O and Ge_2O_2 oxide molecules, whereas the emission of pure germanium clusters dominates under keV ion impact.

A possible way to explain such behavior would be that the signals observed under SHI bombardment originate from electronic sputtering of germanium oxide, remnants of which are present even on the sputter cleaned surface. Since the SHI beam irradiates a larger surface area than the keV ion beam, one might suspect that the signal observed under SHI bombardment may originate from outer parts of the irradiated surface area, which have not been completely cleaned by the preceding keV bombardment. In light of the data presented in Fig. 2, however, we do not expect large signal contributions from these parts of the irradiated surface. To investigate the role of surface contamination further, we have repeated the experiment using the interleaved sputter cleaning technique described in the experimental section. We note that under these conditions the surface is completely amorphized by the continuous keV ion bombardment. Spectra measured on such a dynamically cleaned surface are depicted in Fig. 6.

It is seen that the SHI generated signals now appear reduced with respect to the keV generated signals. In comparing the observed signal levels, it should be noted that the spectra were taken with a significantly reduced SHI pulse particle current of about 1 nA, whereas the keV beam current was increased 1.5-fold with respect to the data presented in the preceding figures. If corrected for this difference, the SHI generated neutral Ge^0 signal is about 5 times higher than that induced by the keV ion impact, which is similar to the ratio derived from the data of Fig. 5. What has changed, however, is the relation between post-ionized neutrals and secondary ions measured under SHI bombardment. In fact, it is evident that now about equal parts of the Ge signal observed in the SNMS spectrum arise from Ge^0 and Ge^+, respectively, while practically all GeO molecules are detected as GeO^+ secondary ions. It is interesting to note that GeO now even appears to represent the majority species in the SHI induced spectra, but the analysis below will show that this impression is misleading.

A quantitative statement with regard to both the composition and the ion fraction of the sputtered material requires information about the a priori unknown photoionization efficiency of the sputtered neutral species. For Ge atoms, we can compare the neutral-to-ion ratio measured here with a similar experiment performed previously in our lab [49]. Using the same ToF spectrometer as applied here, in connection with a more powerful 157 nm laser allowing saturation of the post-ionization efficiency, we measured an ionization probability of the order of 10^{-4} for Ge atoms sputtered from a dynamically cleaned germanium surface under the same bombarding conditions (5 keV Ar^+ ions impinging under 45°) as used here. From the data displayed in Fig. 6 one finds a SIMS/SNMS signal ratio of 1.1×10^{-2} under keV bombardment, indicating that the post-ionization efficiency achieved here is of the order of 1%. The Ge SNMS signal displayed in Fig. 6 is therefore highly underestimated and must in principle be corrected for that efficiency, yielding a corrected SIMS/SNMS ratio of about 5×10^{-3} for Ge atoms sputtered under SHI bombardment. At present, it is unclear what generates the SNMS signal observed for GeO. Looking at the laser intensity dependence of the measured signals, one finds a linear dependence, indicating that the GeO signal must arise from a single photon absorption process. On the other hand, direct single photon ionization of neutral ground state GeO molecules is not possible with our laser wavelength, since the published ionization potential of this molecule (11.1 eV [50]) is significantly higher than the photon energy. The same argument excludes a dissociative ionization of larger clusters like Ge_2O_2 (which are also observed in our spectra). Practically the only

possibility for a GeO^+ signal arising from single photon absorption at 157 nm is a neutral GeO^* precursor molecule which is emitted in a metastable (electronically or vibrationally) excited state. Alternatively, it is possible that the signal is generated via a resonance enhanced two photon ionization process, where the first excitation step is saturated, leading to an apparent single photon absorption behavior.

In any case, the data presented here clearly show that the material emitted from a dynamically sputter cleaned germanium surface under bombardment with $^{197}Au^{26+}$ ions is predominantly neutral and appears to be composed mainly from single Ge atoms. The corresponding signal of Ge^+ ions – albeit detectable – is negligibly small ($\leq 1\%$) compared to that of the emitted neutral atoms. Although not shown here, we note that the signal of negative Ge^- ions measured at the sputter cleaned surface is even smaller, with the corresponding SIMS spectra being dominated by hydrocarbon ion peaks at masses 24 and 27, respectively. These findings clearly underline the necessity of detecting the sputtered neutral particles. In fact, our result of a negligibly small Ge^+ yield is consistent with a similar finding of L'Hoir et al., who investigated the ion emission from a germanium crystal surface under impact of 5.6 MeV/u Pb^{28+} ions and found no evidence of Ge emission [17]. Looking at the secondary ion spectra alone, one might therefore get the erroneous impression that the Ge sample is not being sputtered under these irradiation conditions, while in reality the sputter yield of Ge atoms is relatively large. Even with dynamical sputter cleaning under UHV conditions, there is a sizeable contribution of Ge_xO_y clusters to the sputtered flux, which in our experiments are exclusively detected as secondary ions. Unfortunately, the unknown photoionization efficiency of these clusters precludes a more quantitative estimate of their partial sputter yields.

In summary, we detect an at least 5-fold higher mass spectrometric signal under SHI bombardment as compared to bombarding the same surface with 5 keV Ar^+ ions. For the latter case, it is well known that the emission process is dominated by nuclear sputtering, and the respective sputter yield can be estimated using the SRIM program package, yielding a value of 5.4 atoms/ion, which was also measured experimentally (5.4 ± 0.4 atoms/ion [48]). Using the MeV/keV signal ratio measured here, and correcting for the difference in primary ion current, this would translate to a 5-fold larger sputter yield under SHI bombardment. We wish to note again, however, that care must be taken when interpreting measured SNMS/SIMS data in terms of sputter yields as explained above. Calculating the purely nuclear sputter yield at these energies using SRIM, one obtains a very small value of about 0.26 atoms/ion, which clearly cannot explain the measured mass spectra. Therefore, we conclude that there must be a sizeable – and clearly dominating – electronic sputtering effect when bombarding germanium with 4.8 MeV/u gold ions.

This finding is of interest since it is well known that germanium does not easily form tracks under SHI bombardment [51]. Calculating the electronic stopping power using the CasP program [52] with the default settings[1], one finds dE/dx = 19 keV/nm under 4.8 MeV/u Au^{26+} bombardment. In an attempt to vary the energy deposition density, we have repeated the same experiment using a 4.8 MeV/u $^{48}Ca^{10+}$ ion beam under otherwise identical experimental conditions. The stopping power calculated for this projectile is dE/dx = 3.5 keV/nm. The resulting mass spectra are displayed in Fig. 7. In this experiment, the sample was bombarded with the rastered keV ion beam for about 10 h and then analyzed under interleaved keV sputtering conditions in order to ensure a clean surface. It is clearly seen that under these conditions the spectra generated by the SHI beam are practically empty, although the pulse particle current used here was comparable with that used in the gold experiments. On the other hand, the keV generated spectra reveal that the post-ionization was working properly,

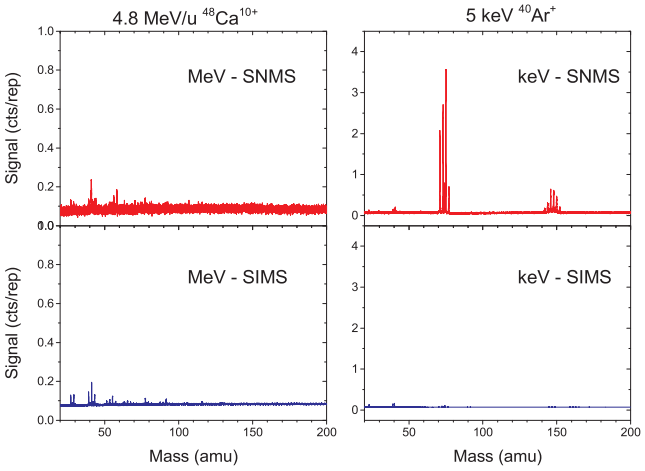

Fig. 7. SNMS and SIMS spectra taken on a dynamically sputter cleaned germanium sample under 4.8 MeV/u $^{48}Ca^{10+}$ impact (left panels) and 5 keV Ar^+ impact (right panels). The sample was pre-bombarded by the rastered Ar^+ ion beam to a total fluence of $> 10^{16}$ ions/cm^2, and the spectra were then taken with interleaved sputter cleaning at about 4×10^{12} ions/cm^{2}s using a pulse particle current of 39 nA (SHI) and 22 nA (Ar^+), respectively.

with a SIMS/SNMS signal ratio of 10^{-2} for the sputtered Ge atoms as shown in Fig. 6. Therefore, we are forced to conclude that the germanium sample is not sputtered by the calcium ion projectiles, thereby clearly indicating that there must be an energy deposition threshold value for the electronic sputtering process observed under gold ion bombardment.

3.3. Ionic crystals

As an example for an ionic crystal, we present data measured on a freshly cleaved potassium bromide sample. This material was chosen, since the ionization potential (IP) of KBr molecules (7.85 eV [50]) is ideally suited for post-ionization with the F_2-Laser (for comparison, LiF molecules have an IP of 11.5 eV [53] and are therefore not easily detectable in our system). Although not known, larger clusters are likely to exhibit smaller ionization potentials, so that we were confident to be able to efficiently photoionize those species as well. In order to avoid charging due to the ion bombardment, the sample was covered with a stainless steel grid (transmission 90%) and then clamped to the sample holder using a molybdenum mask with a 2 mm diameter central aperture. Typical mass spectra obtained for both ion polarities under 4.8 MeV/u $^{197}Au^{26+}$ ion bombardment are shown in Fig. 8. While the positive SNMS and SIMS spectra were acquired simultaneously as described above, the negative SIMS spectrum was measured separately with the polarity of all potentials reversed and the post-ionization laser switched off. In this particular experiment, the laser pulse was temporally shifted with respect to the extraction pulse in order to clearly differentiate between secondary ions and post-ionized sputtered neutrals in the SNMS spectrum as described in the experimental section.

It is seen that both MeV and keV ions induce similar positive secondary ion spectra containing K^+ as the major species, followed by cluster ions like KCO^+, K_2^+ and K_2Br^+ at m/z 67, 78 and 158/160, with the relative intensities of these cluster ions being significantly stronger under SHI impact. The SNMS spectrum generated under SHI bombardment exhibits clear signatures of post-ionized neutral K atoms and K_xBr_y clusters, while the keV induced SNMS spectrum only contains the respective secondary ion signals. At first sight, at least the occurrence of neutral K atoms in the sputtered flux is surprising, since the particles are emitted from an ionic crystal where their equilibrium charge state is positively charged. Therefore, it is well known (and easily understandable) that the alkali constituents of an alkali halide crystal are exclusively knocked off the surface as positive secondary

[1] The calculations were done using the "UCA" model and "charge state scan" screening function

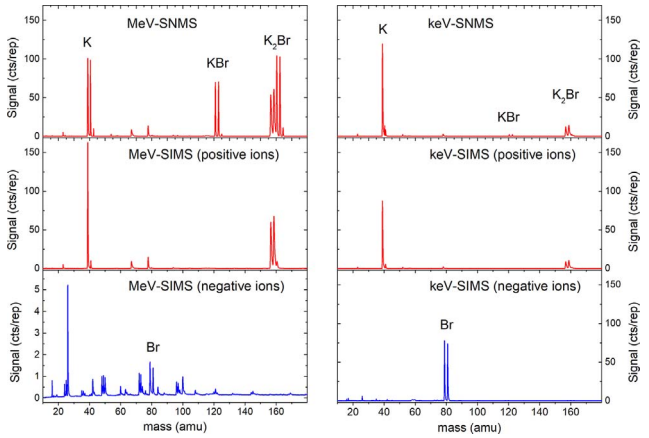

Fig. 8. SNMS (upper panels) as well as positive (middle panels) and negative (bottom panels) SIMS spectra taken on a dynamically sputter cleaned potassium bromide sample under 4.8 MeV/u $^{197}Au^{26+}$ impact (left panels) and 5 keV Ar^+ impact (right panels). The sample was analyzed using a pulse particle current of about 1.7 nA (SHI) and 45 nA (Ar^+), respectively.

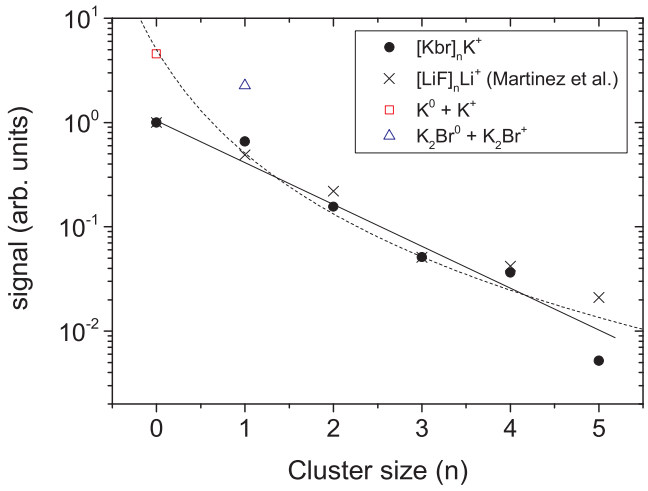

Fig. 9. Integrated signals of $[KBr]_nK^+$ secondary ions as a function of the cluster size n (full black dots). The data were normalized to the K^+ signal at n = 0. For comparison, literature data measured for $[LiF]_nLi^+$ secondary ions sputtered from lithium fluoride under bombardment with 9.1 MeV/u Ge projectiles reproduced from Ref. [22] were included (crosses). Open symbols depict the total integrated SNMS signals (i.e., the sum of post-ionized neutrals and secondary ions) of K and K_2Br, respectively.

ions during the collisional sputtering process induced by keV ion impact. For the same reason, the halogen atoms are expected to be emitted as negatively charged secondary ions. This is clearly observed in the keV generated spectra, where Br^- is detected with comparable intensity as K^+. However, practically no signature of these ions is observed in the SHI-generated negative ion spectrum. Apparently, the SHI impact must trigger a fundamentally different emission process, which leads to the formation and ejection of neutral material, i.e., an effective neutralization of at least the alkali ions on their way to escape into the vacuum. Since the secondary ions are missing, one would expect to find neutral boron atoms in the sputtered flux as well, since the sputtering process must – at least in the limit of large ion fluence – remove the sample material in a stoichiometric way. Unfortunately, our instrument does not allow an efficient detection of neutral B atoms, since their ionization energy of 11.84 eV is significantly above the laser photon energy employed here. We wish to note, however, that we do observe a small signal in the SNMS spectrum which shows the correct isotope distribution of Br and is not observed in the corresponding positive SIMS spectrum, and therefore must be assigned to post-ionized neutral Br atoms. The photoionization process for these atoms must proceed via a non-resonant two photon absorption, which is fairly inefficient at the employed laser intensities.

In any case, the data presented in Fig. 8 indicate that a large fraction – if not the majority – of the neutral material sputtered under SHI impact consists of clusters, a finding which is in pronounced contrast to the keV impact induced sputtering process. Comparing the secondary ion and neutral signals in Fig. 8, one finds that about half of the sputtered K atoms and K_2Br clusters are emitted as positively charged secondary ions, but we have measured other examples where the neutral-to-ion ratio was even larger [44]. As an extreme, KBr molecules, which form about 1/3 of the total observed signal, are exclusively observed in the neutral state. Larger clusters are also observed, predominantly as a series of positive $K_{x+1}Br_x^+$ secondary ions. In a similar fashion, we observe a progression of negative $K_xBr_{x+1}^-$ secondary ions with, however, at least a factor 10 less intensity. Following a suggestion of others [22,39], we interpret these series in the form $[KBr]_nK^+$ and $[KBr]_nBr^-$, thereby basically assuming that a neutral $[KBr]_n$ cluster formed during the emission process becomes ionized by attachment of either a co-sputtered K^+ or Br^- ion. Fig. 9 shows the progression of measured $[KBr]_nK^+$ signals as a function of the cluster size n with the data being normalized to the K^+ signal plotted at $n = 0$. For comparison, we include similar data obtained in Ref. [22] for $[LiF]_nLi^+$ clusters sputtered from lithium fluoride under bombardment with 9.1 MeV/u Ge projectiles. Surprisingly, we find almost the same size distribution with a quasi-exponential decay as observed there (indicated as a straight line in Fig. 9). In connection with the observation that the size distribution – if normalized to the respective value at $n = 0$ – was found to be almost independent of the projectile [22], this observation appears to manifest a universal trend characterizing the cluster formation mechanism during an SHI induced emission process.

However, our data indicate that care must be taken when interpreting the secondary ion spectra in terms of the sputtering and cluster formation processes, since many of the sputtered particles – and particularly single atoms and small clusters – are emitted in the neutral state. Looking at the total detected mass spectrometric signal, i.e., the sum of post-ionized neutrals and secondary ions, we find the values for K ($n = 0$) and K_2Br ($n = 1$) which are depicted as open symbols in Fig. 9. At first sight, it appears as if the same exponential decay could be fitted to these data as well, albeit with about a factor 3 higher signals. However, for all values of $n > 1$ the measured post-ionization signals are below our detection limit and therefore fall by orders of magnitude below this expectation, rendering the signal of post-ionized neutrals negligible compared to the respective secondary ion signal. For $n \geq 2$, the size distribution depicted in Fig. 9 therefore represents that of the total mass spectrometric signals. It is obvious that the yield distribution indicated by these signals now looks different and, in particular, cannot be described by a simple exponential decay any more. In fact, the dashed line included in the figure shows that the distribution can just as well be fitted by a power law decay according to $n^{-\delta}$ with an exponent $\delta \sim 3$. Cluster yield distributions of this kind have been observed many times under keV sputtering conditions [54], where it was also demonstrated that the inclusion of the neutral sputtered material is crucial for the determination of cluster size distributions, since the ionization probability of an emitted cluster may strongly depend on its size.

The data depicted in Fig. 9 also show that the formation of a sputtered $K_{n+1}Br_n^+$ cluster ion does not necessarily proceed via the combination of a neutral $[KBr]_n$ with a K^+ ion. In fact, if this was the case, one would expect to observe a similar progression of neutral $[KBr]_n$ clusters as well [39], which we, however, only see up to $n = 2$. More specifically, the signal observed for $[KBr]_2^0$ is already by a factor of about 30 smaller than that of $[KBr]^0$, while all $[KBr]_n^0$ signals with $n > 2$ fall below our detection limit, indicating a much steeper decay with increasing n than the corresponding $[KBr]_nK^+$ clusters in Fig. 9. Comparing the signals of K_2Br^0 and K_2Br^+, one finds a similar ratio as that between K^0 and K^+, indicating either that also the neutral cluster is

formed via combination of a neutral KBr molecule and a neutral K atom or that both the K^+ and the K_2Br^+ ions are neutralized with about the same efficiency during the sputtering process. Larger clusters, on the other hand, appear to favor the adduction of K^+, indicating that either the neutral $[KBr]_n$ clusters are less stable than their potassium adduct counterparts or that neutralization is less efficient for larger clusters. Another possibility would be that our photoionization process is less efficient for larger clusters, induced either by lower photoabsorption cross sections or by photon induced fragmentation, leading to an underestimation of the neutral $[KBr]_n$ cluster signals in our experiment. Inefficient post-ionization could in principle be induced by ionization potential (IP) values exceeding our laser photon energy. To the best of our knowledge, the exact IP values of $[KBr]_n$ clusters are currently not known. For $n = 1$, the value of 7.85 eV [50] is obviously below our photon energy as mentioned above. For $n \rightarrow \infty$, on the other hand, the IP must converge to that of the KBr solid (7.95 eV [55]), which is slightly above our photon energy of 7.9 eV. Since it has been shown that the effective IP of sputtered clusters is often lowered by the internal energy imparted to the cluster during the sputtering process [56], we believe that inefficient post-ionization is probably not the cause for the observed lack of signal. Clearly, more data are needed to resolve that question, for instance by employing a different post-ionization scheme.

4. Conclusions

The mass spectrometric data presented here clearly show that a large fraction of the material sputtered from a solid surface under irradiation with swift heavy ions is emitted in the neutral state. While this was already known from previous studies employing catcher foils to collect the ejected material, our experiments deliver for the first time a mass resolved comparison of secondary ion and neutral particles, thereby allowing to determine the composition of the sputtered flux and to study the ion fraction of different emitted species separately. We find a significant electronic sputtering process even for some metallic targets, where it is commonly assumed that such effects should be small due to the fast transport of electronic excitation away from the projectile ion trace. For germanium, as an example for a semiconducting target material, we find a huge electronic sputtering effect, which exhibits a clear threshold behavior with respect to the electronic stopping power. For clean metal and semiconductor surfaces, the sputtered flux induced by SHI impact is dominated by the emission of neutral atoms with only negligible ion fraction which, however, appears to be larger than that observed under collisional sputtering conditions induced by keV ion bombardment. Interestingly, a sizeable fraction of the material sputtered from a pristine germanium surface is emitted as neutral GeO or GeOH molecules, indicating that oxide must in some way be involved in the electronic sputtering process. This fraction is reduced but still present – now mostly in form of GeO/H^+ secondary ions - if the surface is thoroughly sputter cleaned during the data acquisition process.

For KBr as an example of an ionic crystal, we find that at least half of the sputtered alkali atoms are emitted in the neutral state. Besides the expected prominent signal of positive alkali ions, we find only negligible emission of the corresponding negative halogen ions. Both findings are fundamentally different from keV impact induced collisional sputtering, where both the sputtered alkali and halogen atoms are exclusively emitted as positive and negative secondary ions, respectively, with comparable intensity. The lack of negative bromine ions in our spectra suggests that there must also be a prominent flux of sputtered neutral Br atoms which, however, cannot be detected very efficiently in our experiment. The occurrence of neutral atoms in the material sputtered from an ionic crystal is intriguing, since both constituents are present as ions in the sample and must therefore somehow be neutralized in the course of the emission process.

Besides the atomic species, we observe a series of sputtered clusters like In_n, Bi_n, Ge_n and K_xBr_y, the intensity of which strongly decays with increasing cluster size. For metal and semiconductor material, we find the cluster yields to be rather small compared to that of the emitted atoms, so that for these species the majority of the sputtered material consists of neutral target atoms. For the ionic crystal, our data indicate that at least half of the sputtered material may be emitted in form of clusters. Here, also, the size distribution is found to decay with increasing cluster size, although the cluster formation and ionization processes are not easy to unravel. Small clusters like KBr and K_2Br are predominantly emitted as neutrals, whereas larger clusters of the type $[KBr]_nK^+$ are exclusively detected as secondary ions. In the negative ion spectra of these materials, we observe a $[KBr]_nBr^-$ series with, however, very small intensity as compared to their positive $[KBr]_nK^+$ counterparts. Both findings support the notion that neutral $[KBr]_n$ clusters formed during the emission process are ionized via K^+- or Br^--adduction, so that one would expect the same cluster size distribution for the emitted neutral clusters as well. Interestingly, however, we do not find those clusters in the post-ionized neutral spectra except at $n = 1$. It remains to be shown in further experiments, whether this is due to an experimental artifact caused by inefficient post-ionization of larger clusters or a characteristic of the electronic sputtering process.

Acknowledgements

The authors are greatly indebted to W. Saure and A. Siegmund for technical assistance during the setup of the experiment. We also acknowledge financial support from the German Ministry of Science (BMBF) in the framework of the Verbundprojekt 05K13PG1 and 05K16PG1 “Ion Induced Materials Characterization and Modification”.

References

[1] Sputtering by Particle Bombardment, Vol. I – IV, in: R. Behrisch et al. (eds.), Topics in Applied Physics Vol. 42, 52, 64 and 110, Springer.
[2] A. Benninghoven, F.G. Rüdenauer, H.W. Werner, Secondary Ion Mass Spectrometry: Basic Concepts, Instrumental Aspects and Trends, Wiley, New York, 1987.
[3] Special issue on fundamental processes in sputtering of atoms and molecules (SPUT92), in: P. Sigmund (ed.), [Mat. Fys. Medd. 43 (1993)].
[4] Ion beam science: solved and unsolved problems, in: Det Kongelige Danske Videnskabernes Selskab, P. Sigmund (ed.), 2006.
[5] W. Assmann, M. Toulemonde, C. Trautmann, Electronic sputtering with swift heavy ions, in: R. Behrisch, W. Eckstein (Eds.), Sputtering by Particle Bombardment, Springer, Berlin, 2007, pp. 401–450.
[6] Z.E. Switkowski, F.M. Mann, D.W. Kneff, R.W. Ollerhead, T.A. Tombrello, New technique for measurement of sputtering yields, Radiat. Eff. Defects Solids 29 (1976) 65–70.
[7] Y. Qiu, I.E. Griffith, T.A. Tombrello, A new technique for measuring sputtering yields at high energies, Nucl. Instrum. Methods B 1 (1984) 118–122.
[8] T.A. Tombrello, Surface modification using mev ion-beams, Nucl. Instrum. Methods 218 (1983) 679–683.
[9] M. Toulemonde, W. Assmann, C. Trautmann, F. Gruner, Jetlike component in sputtering of LiF induced by swift heavy ions, Phys. Rev. Lett. 88 (2002).
[10] H.D. Mieskes, W. Assmann, F. Gruner, H. Kucal, Z.G. Wang, M. Toulemonde, Electronic and nuclear thermal spike effects in sputtering of metals with energetic heavy ions, Phys. Rev. B 67 (2003).
[11] M. Toulemonde, W. Assmann, C. Trautmann, F. Gruner, H.D. Mieskes, H. Kucal, Z.G. Wang, Electronic sputtering of metals and insulators by swift heavy ions, Nucl. Instrum. Methods B 212 (2003) 346–357.
[12] S.A. Khan, A. Tripathi, M. Toulemonde, C. Trautmann, W. Assmann, Sputtering yield of amorphous C-13 thin films under swift heavy-ion irradiation, Nucl. Instrum. Methods B 314 (2013) 34–38.
[13] A. Meftah, W. Assmann, N. Khalfaoui, J.P. Stoquert, F. Studer, M. Toulemonde, C. Trautmann, K.O. Voss, Electronic sputtering of Gd3Ga5O12 and Y3Fe5O12 garnets: yield, stoichiometry and comparison to track formation, Nucl. Instrum. Methods B 269 (2011) 955–958.
[14] M. Toulemonde, W. Assmann, C. Trautmann, Electronic sputtering of vitreous SiO2: experimental and modeling results, Nucl. Instrum. Methods B 379 (2016) 2–8.
[15] M. Toulemonde, W. Assmann, D. Muller, C. Trautmann, Electronic sputtering of LiF, CaF2, LaF3 and UF4 with 197MeV Au ions. Is the stoichiometry of atom emission preserved? Nucl. Instrum. Methods B (2016).
[16] M.R. Weller, K.M. Hubbard, R.A. Weller, D.L. Weathers, T.A. Tombrello, Sticking probabilities for sputtered ag and au atoms incident on oxidized aluminum surfaces, Nucl. Instrum. Methods B 42 (1989) 19–28.
[17] A. L'Hoir, C. Koumeir, S. Della Negra, P. Boduch, P. Roussel-Chomaz, A. Cassimi, M. Chevallier, C. Cohen, D. Dauvergne, M. Fallavier, D. Jacquet, B. Manil, J.C. Poizat, C. Ray, H. Rothard, D. Schmaus, M. Toulemonde, Study of ion emission from a germanium crystal surface under impact of fast Pb ions in channeling conditions, Nucl. Instrum. Methods B 267 (2009) 876–880.

[18] H. Hijazi, H. Rothard, P. Boduch, I. Alzaher, F. Ropars, A. Cassimi, J.M. Ramillon, T. Been, B.B. d'Etat, H. Lebius, L.S. Farenzena, E.F. da Silveira, Interaction of swift ion beams with surfaces: sputtering of secondary ions from LiF studied by XY-TOF-SIMS, Nucl. Instrum. Methods B 269 (2011) 1003–1006.
[19] H. Hijazi, L.S. Farenzena, H. Rothard, P. Boduch, P.L. Grande, E.F. da Silveira, Cluster ion emission from LiF induced by MeV Nq+ projectiles and 252Cf fission fragments, Eur. Phys. J. D 63 (2011) 391–400.
[20] H. Hijazi, H. Rothard, P. Boduch, I. Alzaher, A. Cassimi, F. Ropars, T. Been, J.M. Ramillon, H. Lebius, B. Ban-d'Etat, L.S. Farenzena, E.F. da Silveira, Electronic sputtering: angular distributions of (LiF)nLi+ clusters emitted in collisions of Kr (10.1 MeV/u) with LiF single crystals, Eur. Phys. J. D 66 (2012) 68.
[21] H. Hijazi, T. Langlinay, H. Rothard, P. Boduch, F. Ropars, A. Cassimi, L.S. Farenzena, E.F. da Silveira, Strong perturbation effects in heavy ion induced electronic sputtering of lithium fluoride, Eur. Phys. J. D 68 (2014) 185.
[22] R. Martinez, L. Th, P. Boduch, A. Cassimi, H. Hijazi, F. Ropars, P. Salou, E.F.D. Silveira, H. Rothard, Electronic sputtering of thin lithium fluoride films induced by swift heavy ions, Mater. Res. Exp. 2 (2015) 076403.
[23] W. Assmann, B. Ban-d'Etat, M. Bender, P. Boduch, P.L. Grande, H. Lebius, D. Lelievre, G.G. Marmitt, H. Rothard, T. Seidl, D. Severin, K.O. Voss, M. Toulemonde, C. Trautmann, Charge-state related effects in sputtering of LiF by swift heavy ions, Nucl. Instrum. Methods B 392 (2017) 94–101.
[24] M.G. Blain, E.A. Schweikert, E.F. Da Silveira, Clusters as projectiles for SIMS, J. Phys.-Paris 50 (1989) C2–C85.
[25] C.C. de Castro, I.S. Bitensky, E.F. da Silveira, Desorption of H- ions from solid surfaces induced by MeV ion impact, Nucl. Instrum. Methods B 132 (1997) 561–570.
[26] J.A.M. Pereira, E.F. Da Silveira, K. Wien, MeV nitrogen bombardment of LiF: from the nuclear to the electronic sputtering regimes, Radiat. Eff. Defects Solids 142 (1997) 247–255.
[27] E.F. Da Silveira, S.B. Duarte, E.A. Schweikert, Multiplicity analysis: a study of secondary particle distribution and correlation, Surf. Sci. 408 (1998) 28–42.
[28] J.A.M. Pereira, E.F. Da Silveira, Li/sup +/ secondary ion energy distributions probed by fast N/sub 2//sup +/ and N/sup q+/ bombardment of LiF, Nucl. Instrum. Methods B 146 (1998) 185–189.
[29] J.A.M. Pereira, I.S. Bitensky, E.F. da Silveira, Effects of charge state and number of constituents of MeV projectiles on secondary ion emission yields from LiF, Nucl. Instrum. Methods B 135 (1998) 244–249.
[30] C.C. de Castro, I.S. Bitensky, E.F. da Silveira, M. Most, K. Wien, Energy distribution of H+ ions desorbed from metal surfaces by MeV ion impact, Int. J. Mass Spectrom. 173 (1998) 1–15.
[31] J.A.M. Pereira, E.F. da Silveira, Li+ secondary ion energy distributions probed by fast N2+ and Nq+ bombardment of LiF, Nucl. Instrum. Methods B 146 (1998) 185–189.
[32] J.A.M. Pereira, I.S. Bitensky, E.F. da Silveira, Nonlinear effects in ion emission from LiF induced by N+ and N-2(+) MeV ion impact, Int. J. Mass Spectrom. 174 (1998) 179–191.
[33] J.A.M. Pereira, E.F. da Silveira, Combined TOF-MS/RBS analysis of LiF thin films bombarded by MeV nitrogen ions, Nucl. Instrum. Methods B 136 (1998) 779–783.
[34] J.A.M. Pereira, E.F. da Silveira, Li+ secondary ion energy distributions probed by fast N-2(+) and Nq+ bombardment of LiF (vol 146, pg 185, 1998), Nucl. Instrum. Methods B 155 (1999) 206.
[35] J.A.M. Pereira, E.F. da Silveira, Cluster and velocity effects on yields and kinetic energy distributions of Li+ desorbed from LiF, Phys. Rev. Lett. 84 (2000) 5904–5907.
[36] T. Jalowy, R. Neugebauer, M. Hattass, J. Fiol, F. Afaneh, J.A.M. Pereira, V. Collado, E.F. da Silveira, H. Schmidt-Bocking, K.O. Groeneveld, Dynamics of secondary ion emission: novel energy and angular spectrometry, Nucl. Instrum. Methods B 193 (2002) 762–767.
[37] T. Jalowy, R. Neugebauer, K.O. Groeneveld, C.R. Ponciano, L.S. Farenzena, E.F. da Silveira, XY-TOF technique for large ion source mass spectrometers, Int. J. Mass Spectrom. 219 (2002) 343–350.
[38] F. Alberto, O.P. Fernandez-Lima, A. Vilela Neto, M.A.C Silva Pimentel, C.R. Pacheco, M.A.C Nascimento, E.F. da Silveira, Theoretical and experimental study of negative LiF clusters produced by fast ion impact on a polycrystalline 7LiF target, J. Phys. Chem. A 113 (2009) 15031–15040.
[39] F.A. Fernandez-Lima, O.P. VilelaNeto, A.S. Pimentel, C.R. Ponciano, M.A.C. Pacheco, M.A.C. Nascimento, E.F. de Silveira, A theoretical and experimental study of positive and neutral LiF clusters produced by fast ion impact on a polycrystalline LiF target, J. Phys. Chem. A 113 (2009) 1813–1821.
[40] P. Iza, L.S. Farenzena, T. Jalowy, K.O. Groeneveld, E.F. da Silveira, Secondary ion emission dynamics model: a tool for nuclear track analysis, Nucl. Instrum. Methods B 245 (2006) 61–66.
[41] R.A. Weller, T.A. Tombrello, Energy-spectra of sputtered U-235 atoms, Bull. Am. Phys. Soc. 23 (1978) 102-102.
[42] R.A. Weller, T.A. Tombrello, Energy-spectrum of sputtered uranium - new technique, Radiat. Eff. Defects Solids 37 (1978) 83–92.
[43] A. Wucher, Laser postionization – fundamentals, in: J.C. Vickerman, D. Briggs (Eds.), TOF-SIMS: Materials Analysis by Mass Spectrometry, IM Publications and Surface Spectra, 2013, pp. 217–246.
[44] F. Meinerzhagen, L. Breuer, H. Bukowska, M. Herder, M. Bender, D. Severin, H. Lebius, M. Schleberger, A. Wucher, SHIPS: a new setup for the investigation of swift heavy ion induced particle emission and surface modifications, Rev. Sci. Instrum. 87 (2016).
[45] M. Toulemonde, Irradiation by swift heavy ions: influence of the non-equilibrium projectile charge state for near surface experiments, Nucl. Instrum. Methods B 250 (2006) 263–268.
[46] www.srim.org.
[47] L. Breuer, F. Meinerzhagen, M. Herder, M. Bender, D. Severin, J.O. Lerach, A. Wucher, Secondary ion and neutral mass spectrometry with swift heavy ions: organic molecules, J. Vac. Sci. Technol., B 34 (2016) 03H130.
[48] R. Heinrich, A. Wucher, Yields and energy distributions of sputtered semiconductor clusters, Nucl. Instrum. Methods B 140 (1998) 27–38.
[49] R. Heinrich, C. Staudt, M. Wahl, A. Wucher, Ionization Probability of Sputtered Clusters, Elsevier Science (1999) pp. 111–114.
[50] K.P. Huber, G. Herzberg, Molecular Spectra and Molecular Structure. IV. Constants of Diatomic Molecules, Van Nostrand Reinhold Company Inc., New York, 1979.
[51] A. Kamarou, W. Wesch, E. Wendler, A. Undisz, M. Rettenmayr, Radiation damage formation in InP, InSb, GaAs, GaP, Ge, and Si, due to fast ions, Phys. Rev. B 78 (2008).
[52] http://www.casp-program.org.
[53] V.G. Zakzhevskii, Features of a theoretical description of ionization potentials of the LiF molecule and electron affinity of the F atom, Theoret. Exp. Chem. 26 (1991) 676–679.
[54] A. Wucher, M. Wahl, Cluster Emission in Sputtering, Wiley & Sons, 1995, pp. 65-72.
[55] B.L. Henke, J. Liesegang, S.D. Smith, Soft-x-ray-induced secondary-electron emission from semiconductors and insulators: models and measurements, Phys. Rev. B 19 (1979) 3004–3021.
[56] A. Wucher, C. Staudt, S. Neukermans, E. Janssens, F. Vanhoutte, R.E. Silverans, P. Lievens, On the internal energy of sputtered clusters, New J. Phys. 10 (2008) 1–22.